Available online at www.sciencedirect.com

ScienceDirect

Proceedings of the Combustion Institute 000 (2022) 1–10

Proceedings of the Combustion Institute

www.elsevier.com/locate/proci

Wall heat transfer and flame structure transitions in stagnating spray flames

Danyal Mohaddes*, Matthias Ihme

Department of Mechanical Engineering, Stanford University, Stanford, California 94305, United States

Received 5 January 2022; accepted 8 August 2022
Available online xxx

Abstract

Wall-stagnating spray flames are of importance in a number of engineering applications, including accidental leakage of liquid fuel from pressurized fuel lines as well as in direct-injected compression and spark-ignition engines. The wall heat flux generated by such flames is an important consideration in the design and analysis of affected components. To identify and analyze the key parametric dependencies of the flame structure and wall heat flux, we carry out one-dimensional simulations of wall-stagnating spray flames employing an Eulerian-Eulerian formulation and a realistic 54-species chemical mechanism for *n*-dodecane/air combustion. Conjugate heat transfer is accounted for by considering a finite-thickness wall. We find that the configuration permits three distinct flame structures, namely wall-stabilized, detached, and injector-stabilized flames. Since the near-wall flame structure determines the wall heat flux, the parameter space is explored to identify points of flame structure transition. We show that the Stokes number and the liquid mass loading play a key role in controlling the transition in the flame structure and its non-linear coupling to the wall heat flux, the former parameter by controlling the droplet evaporation time and the latter by affecting the amount of fuel able to penetrate the flame. The wall boundary temperature has a direct effect on the wall heat flux, and we show that it exhibits hysteresis in flame structure transition, with an associated change in wall heat flux of up to 30 percent.

Keywords: Spray combustion; Flame-wall interaction; Wall heat transfer

1. Introduction

The structure and associated wall heat flux of stagnating spray flames is of importance to design and analysis in a variety of engineering contexts involving liquid fuels. In many industries, the supply of liquid fuel via pressurized lines near components at elevated temperatures is a safety concern, since a small fuel leakage can impinge on a nearby hot surface. The risk of a fuel leakage event resulting in ignition has thus received significant attention [1,2]. However, once ignition occurs, the relevant quantity of interest is the wall heat flux imparted by the flame to the wall and sustained over long time scales, as this has consequences for the structural

* Corresponding author, currently at FM Global Research.
E-mail address: danyal.mohaddes@fmglobal.com (D. Mohaddes).

https://doi.org/10.1016/j.proci.2022.08.037
1540-7489

integrity and operability of adjacent components. A related problem exists in direct-injected internal combustion engines, where the wall heat flux associated with the interaction of the spray flame with the cylinder liner (or piston bowl) has a significant effect on pollutant formation [3,4].

Flame-wall interaction is a topic of considerable scientific inquiry [5] and has been studied in the head-on quenching (HOQ) configuration using gas-phase wall-stagnating flames [6]. A number of results from this gas-phase literature are relevant to the present study of wall-stagnating spray flames. Specifically, detailed experimental studies of premixed methane/air flames by Mann et al. [7] demonstrated that wall-stagnating flames were largely planar and exhibited little radial variation in either temperature or species profiles, nor consequently in wall heat flux. A recent numerical study of HOQ of a methane/air mixture by Luo et al. [6] showed that increased strain rate and wall temperature increased and diminished wall heat flux, respectively. Wehrfritz et al. [4] performed a numerical study considering parametric variations of equivalence ratio and strain rate in a prevaporized *n*-dodecane/air wall-stagnating flame. The authors showed that the wall heat flux reached a maximum at near-stoichiometric conditions and strain rates close to the extinction limit.

Although spray combustion is less often studied in the wall-stagnating configuration, extensive studies in the counterflow configuration, where the fuel spray is carried by air in one stream against an opposing air stream, have demonstrated a rich variety of flame characteristics [8]. Two distinct flames have been shown to form for sufficiently large droplets [9]. Specifically, large droplets penetrate the partially premixed 'fuel-side' flame and continue vaporizing in the hot product gases, forming an 'oxidizer-side' diffusion flame where the fuel vapor meets the air of the opposing stream. Spray-flame interaction, i.e., the simultaneous effects of fuel vapor addition and sensible enthalpy reduction on combustion chemistry due to spray evaporation, have been shown to result in a number of different flame structures [10]. Flame structures have been shown to exhibit bifurcations through both laminar one-dimensional [11] and turbulent three-dimensional [12] studies.

The steady counterflow spray flame literature has shown that spray evaporation and spray-flame interaction have a first-order effect on the flame structure [10]. Since the near-wall flame structure ultimately determines the wall heat flux, assuming the spray to be prevaporized as has been previously considered [4] neglects important features of the flame. The present study addresses this gap in the literature by performing simulations of wall-stagnating spray flames using realistic models for spray evaporation and combustion chemistry as well as the consideration of conjugate heat transfer in a finite-thickness wall, identifying key parametric dependencies of wall heat flux and analyzing these dependencies in the context of the spray flame structure. To this end, we consider a one-dimensional multiphase stagnation flame coupled to a conjugate heat transfer solver. The problem configuration and mathematical formulation are discussed in Section 2. Wall-stagnating spray flame simulation results are presented and discussed in Section 3. The manuscript closes with conclusions in Section 4.

2. Methodology

The configuration considered is that of a laminar, wall-stagnating multiphase flow at ambient atmospheric pressure, shown in Fig. 1. Steady-state conditions are considered, as this is most relevant for the long time scales the aviation industry considers for component damage due to direct interaction with a flame [13]. We employ *n*-dodecane as a neat surrogate for kerosene-based fuels. Air and *n*-dodecane droplets have equal initial axial velocity $u^* = u_d^*$, scaled radial velocity $V^* = V_d^* = 0$ and temperature $T^* = T_d^*$, where asterisks indicate dimensional quantities and the subscript d refers to liquid-phase quantities, respectively. The spray is modeled as monodisperse. Droplets have an initial mass m_d^* and are injected with a liquid-to-air mass ratio Z_l. The multiphase flow is convected a distance L^* from an injector toward a wall with interface temperature $T^* = T_s^* = T_w^*$, where the subscripts s and w refer to solid-phase quantities and quantities evaluated at the fluid-solid interface, respectively. As in previous studies of wall-stagnating flames [4,6], the wall is taken as chemically inert. The wall has finite thickness L_s^* and external temperature $T_s^* = T_e^*$.

We model the gaseous phase by considering mass, momentum, energy and species conservation equations for chemically reacting flows in axisymmetric cylindrical coordinates along the $(x, r = 0)$ axis, applying conventional assumptions for stagnation flows [9,14]. We consider a multicontinuum, i.e., Eulerian-Eulerian approach to describe the dilute monodisperse spray phase, solving equations for droplet mass, momentum, energy and number density. The system is two-way coupled

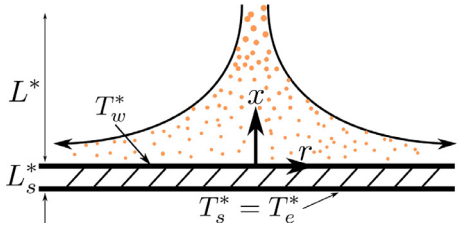

Fig. 1. Wall-stagnating spray flame configuration.

Please cite this article as: D. Mohaddes and M. Ihme, Wall heat transfer and flame structure transitions in stagnating spray flames, Proceedings of the Combustion Institute, https://doi.org/10.1016/j.proci.2022.08.037

for all conserved quantities, with inter-phase exchanges occurring due to evaporation, drag forces and heat transfer. The governing equations for gas and liquid phases were stated and described thoroughly by Franzelli et al. [14]. Evaporation is considered using the Abramzon-Sirignano model, discussed in the context of the one-dimensional formulation by Darabiha et al. [15].

To consider inter-phase heat transfer through the fluid-solid boundary, we augment the governing equations by solving an energy equation in the solid phase. It has been demonstrated through detailed experiments that axial wall heat transfer is dominant in stagnation flames [7]. Heat transfer in the solid phase is thus modeled by the one-dimensional energy equation $0 = d^2T_s^*/dx^{*2}$. The solid and fluid phases are coupled by enforcing the fluid-phase wall heat flux $\dot{q}_w^*$ as a Neumann boundary condition in the solid phase, and the solid-phase wall temperature $(T_s^*)_w$ as a Dirichlet boundary condition in the fluid phase, as suggested by Radenac et al. [16], with both quantities matched in both phases in the steady-state solution. Since the solution in the solid phase is linear, $(T_s^*)_w$ is evaluated analytically as $(T_s^*)_w = T_e^* + L_s^*\dot{q}_w^*/\lambda_s^*$, where λ_s^* is the solid-phase thermal conductivity.

Dimensional reference quantities evaluated at the inlet of the domain are temperature $T^* = 400\,\mathrm{K}$, gas-phase dynamic viscosity $\mu^* = 2.3 \times 10^{-5}\,\mathrm{Pa{\cdot}s}$, isobaric heat capacity $c_p^* = 1.02\,\mathrm{kJ/(kg{\cdot}K)}$, thermal conductivity $\lambda^* = 3.29 \times 10^{-2}\,\mathrm{W/(m{\cdot}K)}$, density $\rho^* = 0.878\,\mathrm{kg/m^3}$ and mixture-averaged diffusivity of fuel vapor into air $\mathcal{D}^* = 8.66 \times 10^{-6}\,\mathrm{m^2/s}$. Other reference quantities are the fluid convective length $L^* = 20\,\mathrm{mm}$, liquid density $\rho_l^* = 669.4\,\mathrm{kg/m^3}$, heat of vaporization $K_v^* = 256.2\,\mathrm{kJ/K}$, solid thickness $L_s^* = 6.35\,\mathrm{mm}$, solid thermal conductivity $\lambda_s^* = 16.2\,\mathrm{W/(m{\cdot}K)}$, and the characteristic reaction rate $\dot{\omega}^* = \dot{\omega}_{\mathrm{CO}}^* + \dot{\omega}_{\mathrm{CO_2}}^* + \dot{\omega}_{\mathrm{H_2}}^* + \dot{\omega}_{\mathrm{H_2O}}^* = 773.0\,\mathrm{kg/(m^3{\cdot}s)}$, taken as the maximum reaction rate of the progress variable for a stoichiometric free flame with unburned temperature T^*. Key time scales in the system are the convective time scale $\tau_f^* = 1/a^*$, where $a^* = u^*/L^*$ is the global strain rate; droplet relaxation time scale $\tau_d^* = \rho_l^* d^{*^2}/(18\mu^*)$, where the droplet diameter d^* is obtained from $m_d^* = \pi\rho_l^* d^{*^3}/6$; and chemical time scale $\tau_c^* = \rho^*/\dot{\omega}^*$.

We perform our analysis in a non-dimensional setting, employing the non-dimensionalization of the governing equations [14] derived by Xie et al. [11]. Dimensionless groups are the Prandtl number $\mathrm{Pr} = \mu^* c_p^*/\lambda^*$; Schmidt number $\mathrm{Sc} = \mu^*/\rho^*\mathcal{D}^*$; Jakob number $\mathrm{Ja} = c_p^* T^*/K_v^*$; Damköhler number $\mathrm{Da} = \tau_f^*/\tau_c^*$, Stokes number $\mathrm{St} = \tau_d^*/\tau_f^*$ and ratio of thermal conductivities $r_\lambda = \lambda^*/\lambda_s^*$. Non-dimensional groups evaluated from reference quantities are $\mathrm{Pr} = 0.72$, $\mathrm{Sc} = 3.03$, $\mathrm{Ja} = 1.60$ and $r_\lambda = 2.03 \times 10^{-3}$. The values of Da, St, $\phi_0 = Z_l/f_{st}$ and T_e are varied independently using numerical continuation to investigate their effects on the flame physics, where ϕ_0 is the total equivalence ratio and $f_{st} = 0.0671$ is the stoichiometric mass ratio for *n*-dodecane/air combustion. The ranges chosen for the non-dimensional parameters in the ensuing analysis correspond to fuel line pressures of 2 bar to 10 bar, leakage orifice diameters of 10^{-5} m to 10^{-4} m, fuel line-to-wall distances of 10^{-2} m to 10^{-1} m and surface temperatures of 600 K to 1200 K. These values are chosen to be representative of the wide range of conditions encountered in aircraft safety applications.

Given that the present formulation allows for spray-gas slip, the largest value of St considered in this study is limited to cases where the spray has fully evaporated prior to reaching the wall. This precludes considerations that arise in the modeling of direct spray-wall interactions in a multi-continuum formulation, which are more accurately captured in a 3D Eulerian-Lagrangian formulation [2].

The governing equations are solved using a modified implementation of the Cantera [17] one-dimensional steady flame solver, which was augmented to consider spray combustion and conjugate heat transfer. In a study of laminar gas-phase wall-stagnating flames [18], results of Cantera simulations were compared directly with centerline experimental results. Close agreement was achieved for temperature and minor species concentrations.

The chemical source terms are computed using a skeletal chemical mechanism for *n*-dodecane/air combustion accounting for both low and high-temperature chemistry [19]. The mechanism consists of 54 species and 269 reactions, and was validated across a wide range of pressures, temperatures and equivalence ratios using experimental measurements and comparisons to detailed mechanisms. It has been applied previously in simulations of prevaporized wall-stagnating flames [4] and hot surface ignition of wall-stagnating fuel sprays [2].

3. Results

We consider wall-stagnating spray flames formed by the flow of monodisperse *n*-dodecane droplets and air against a hot surface of finite thickness. In this study, we discuss the wall heat flux using the wall Nusselt number $\mathrm{Nu}_w = (d_x T)_w/(T_w - 1)$. We also define a spray penetration distance $\ell_p = \ell_F - \ell_d$, where $\ell_F = \arg\max_x(T)$ is the flame's axial position and $\ell_d = \arg\min_x(m_d)$ is the edge of the spray; $\ell_p > 0$ indicates the spray has penetrated the flame. Liquid-phase results will only be plotted for the portion of the domain $x > \ell_d$ where $m_d > 0$.

Please cite this article as: D. Mohaddes and M. Ihme, Wall heat transfer and flame structure transitions in stagnating spray flames, Proceedings of the Combustion Institute, https://doi.org/10.1016/j.proci.2022.08.037

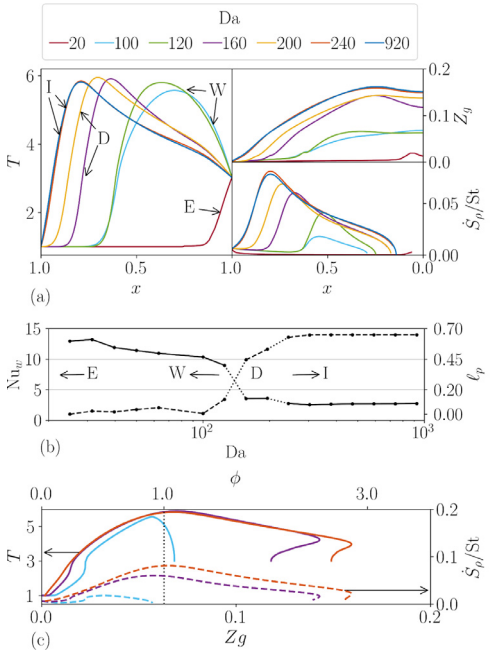

Fig. 2. Parametric dependence on Da, for St = 0.2, ϕ_0 = 1.3 and T_e = 3.0. (a) Flame structure variation in physical space; (b) Nu_w (solid line) and ℓ_p (dashed line), with transitions between regimes shown by dotted lines; (c) flame structure in composition space, with the vertical dotted black line indicating the stoichiometric condition.

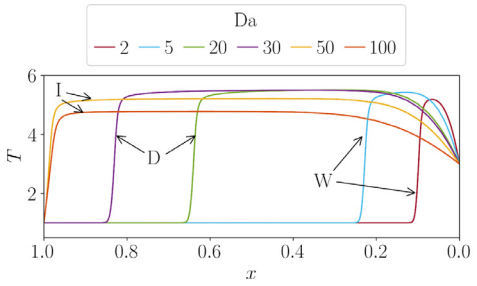

Fig. 3. Parametric dependence on Da for gaseous flames, i.e., St → 0, with ϕ_0 = 1.3 and T_e = 3.0.

3.1. Parametric analysis

We consider first the variation of Da across two orders of magnitude and its resulting effect on flame structure and wall heat flux in Fig. 2, holding all other parameters constant at St = 0.2, T_e = 3.0, and ϕ_0 = 1.3. Three regimes of flame stabilization are accessed in the range of Da considered. These regimes of flame stabilization have been observed through strain rate variations in stagnating gaseous flames [20]. We include results for prevaporized, premixed gaseous flames in Fig. 3 for comparison to the spray flame results. We introduce the regimes of flame stabilization here through Da variation to demonstrate the similarity to the gas-phase flame behavior, before discussing parametric variations and physics specific to stagnating spray flames.

High values of Da result in injector-stabilization, labeled 'I' in Figs. 2 and 3, where the flame is anchored on the injector. The injector boundary is specified as isothermal and is not affected by the flame. In this regime, the injector incurs a non-negligible heat flux from the flame, as can be seen from the gas-phase temperature profile in the left panel of Fig. 2b. The flame location and wall heat flux remain nearly constant, as identified from the peak temperature and from the solid line in Fig. 2b, respectively. In the spray flames, spray evaporation begins immediately after injection, but spray penetration of the flame is substantial, with the spray mass source term remaining significant from the injector to near the wall, shown in the lower right panel of Fig. 2b. The spray mass source term, as it appears in the governing equations [14], is non-dimensionalized to $\dot{S}_\rho$/St, where $\dot{S}_\rho = -n_l \dot{m}_d$, $n_l = \rho Z_l / m_d$ is droplet number density and $\dot{m}_d$ droplet evaporation rate. The Bilger mixture fraction Z_g consequently increases monotonically throughout most of the domain, shown in the upper right panel.

Reducing Da below approximately 220 causes the spray flame to transition and detach from the injector, labeled 'D' in Fig. 2. In this regime the flame is similar to a freely-propagating configuration and responds to parametric variations by changing position, with lower values of Da resulting in the flame stabilizing nearer to the wall. The same transition occurs at a Da value of approximately 40 in the gaseous flame. The flame position is thus indicative of the consumption speed, since in the unburned outer flow, the gas-phase axial velocity decreases linearly from the injector toward the wall. In the spray flame, upstream of the flame location, the spray mass source term remains small and Z_g consequently remains near zero. Once droplets reach the flame, they quickly reach saturation and $\dot{S}_\rho$ rises to its peak value. Considering the results for temperature in composition space in Fig. 2c, we find that the injector-stabilized and detached spray flames have a structure resembling that of a diffusion flame. In these high-Da regimes, once sufficient fuel is vaporized, the flame is established at the stoichiometric condition, with substantial spray evaporation across compositions. The resemblance to a diffusion flame structure is due primarily to the increase in evaporation rate with temperature across the flame, shown in Fig. 2c.

Reduction to Da ≈ 140 results in the spray flame transitioning to the wall-stabilized regime, labeled 'W' in Fig. 2. This transition occurs at a Da value of approximately 10 in the gaseous flame. This transition in topology causes a substantial increase in the wall heat flux, as seen

Please cite this article as: D. Mohaddes and M. Ihme, Wall heat transfer and flame structure transitions in stagnating spray flames, Proceedings of the Combustion Institute, https://doi.org/10.1016/j.proci.2022.08.037

in Fig. 2b. Wall heat flux continues to increase with decreasing Da until extinction, which is in agreement with the established behavior of gas-phase stagnating flames [4]. Extinction is labeled 'E' in Fig. 2, occurring at Da = 20 for the spray flame. The results in composition space show that the wall-stabilized spray flames have a partially-premixed structure. Composition is limited to fuel-lean and near-stoichiometric values, with significantly lower temperatures and spray evaporation rates at highly fuel-lean compositions compared to the other regimes shown. Furthermore, we observe that in the wall-stabilized regime $\ell_p < 0.1$, with substantially less spray penetration of the flame than in the detached and injector-stabilized regimes, where $\ell_p > 0.4$. Thus, despite the ratio of convective and droplet relaxation time scales being held constant through St in the spray flame, we find an important coupling of the spray vaporization and the spray flame behavior across regime transitions.

The variation in ℓ_p and $\dot{S}_\rho$ within the regimes of flame stabilization and across their transitions indicates that spray evaporation behavior has an important role in determining the spray flame topology and consequently the wall heat flux – considerations which are not present in gas-phase flames. We therefore consider the effect of the Stokes number on the flame structure and wall heat flux in detail in Fig. 4, while holding other parameters constant at Da = 100, $\phi_0 = 1.3$ and $T_e = 3.0$. We note that varying St independently of Da has the effect of varying the Lefebvre number $\mathrm{Lf} = \tau_e^*/\tau_c^*$, where τ_e^* is the characteristic droplet evaporation time scale, since $\tau_e^* \sim \tau_d^*$ and thus $\mathrm{Lf} \sim \mathrm{Da\,St}$ [21].

Gas-phase temperature, shown in the left panel of Fig. 4a, shows that varying St results in a traversal of the flame stabilization regimes identified above through Da-variation. Low values of St < 0.06 result in injector stabilization, where the temperature profile indicates flame anchoring. In this regime, the droplet relaxation time scale is small compared to that of convection, and the solution thus approaches the topology of a prevaporized gaseous flame downstream of the injector. The lower-right panel of Fig. 4a demonstrates this point clearly, where for St = 0.02 it is seen that the peak vaporization rate occurs near $x = 0.95$, with the spray fully vaporized by $x = 0.9$. This is a key difference from the injector-stabilized regime observed at high values of Da in Fig. 2a, where spray penetration of injector-stabilized flames extends to near the wall. Considering Fig. 4b, we find that increasing St results in a small increase in ℓ_p and a 30% increase in Nu_w across the injector-stabilized range considered. Increasing St results in larger time scales associated with droplet heating and evaporation, which delays the formation of the flame. The delayed formation of the flame results in a reduced thermal gradient at the injector, and the associated reduction in heat loss to the injector re-

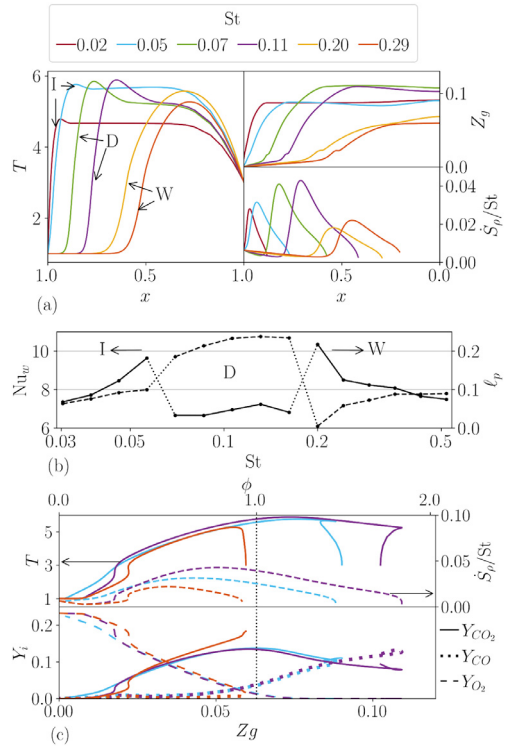

Fig. 4. Parametric dependence on St, for Da = 100, $\phi_0 = 1.3$ and $T_e = 3.0$. (a) Flame structure variation in physical space; (b) Nu_w (solid line) and ℓ_p (dashed line), with transitions between regimes shown by dotted lines; (c) results in composition space, with the vertical dotted black line indicating the stoichiometric condition.

ϕ_0 is constant, the total heat loss to spray evaporation is unchanged. The higher peak temperature thus results in a greater wall heat flux.

Increasing St beyond 0.06 and thereby further increasing the delay in spray evaporation results in a transition in flame topology to the detached regime. As was the case in the context of Fig. 2, in this regime the flame responds to parametric variation by changing position. In the present case, the increased droplet time scale is balanced by the shift in flame position to locations of greater residence time. This can also be viewed as a decrease in the flame consumption speed, resulting in stabilization closer to the wall where gas-phase axial velocity is lower. Peak gaseous temperature and consequently Nu_w remains nearly constant, until the flame transitions to the wall-stabilized regime at St = 0.18. We observe in Fig. 4b that ℓ_p drops from 0.22 to near zero across this transition and subsequently increases in the range considered. We also observe that Nu_w increases by 40% across the transition, and then decreases with increasing St. Similar mechanisms are at play in determining the wall heat flux of the injector and wall-stabilized

Please cite this article as: D. Mohaddes and M. Ihme, Wall heat transfer and flame structure transitions in stagnating spray flames, Proceedings of the Combustion Institute, https://doi.org/10.1016/j.proci.2022.08.037

regimes. In the former, increased St delays establishment of the reaction zone. This pushes the flame downstream, reducing heat losses to the injector and thereby increasing the heat flux on the stagnation wall. In the latter, increased St forces the reaction zone closer to the wall, but in this case the coupled effects of wall heat loss and spray penetration cause a reduction in peak temperature and wall heat flux. Further increasing St beyond the range shown ultimately results in extinction, but these results are not shown as the present formulation is not suitable for analysis in the St $\sim$ 1 regime, as noted in Section 2.

The dependence of the spray flame topology on St demonstrates why it was found that when Da was varied parametrically, the topology transitions of the gaseous flame occurred at lower values of Da compared to the spray flame for equal values of ϕ_0 and T_e. At low values of St, we found that the flame approaches a prevaporized structure and results in the flame anchoring at the injector. In the gaseous flame, the inflow stream is fully prevaporized, and thus also tends to anchor at the injector. Achieving topology transition away from the injector and into the detached and wall-stabilized regimes thus requires higher strain rates, i.e., lower values of Da. Hence, the same topology transitions are observed in Figs. 2 and 3, but in Fig. 3 they occur at lower values of Da.

In Fig. 4c, we consider the flame structures in composition space. The top panel of the figure shows that the wall-stabilized flame exhibits a partially-premixed structure limited to fuel-lean compositions. The detached and injector-stabilized flames have structures comparable to results shown in Fig. 2c. However, unlike the behavior observed in varying Da, we find that the changes in composition with St are non-monotonic: the largest values of Z_g are reached in the detached rather than injector-stabilized flame regime. In the lower panel of Fig. 4c we analyze the differences in chemical composition of flames across regimes. For all flame structures, oxygen is almost entirely consumed at fuel-lean values of Z_g. Compared to the detached and injector-stabilized flame structures, the wall-stabilized flame results in much higher combustion efficiency, with little production of CO. The structures obtained at lower values of St are seen to produce approximately equal mass fractions of CO and CO_2, with most CO production occurring at fuel-rich compositions. We note that although the inflow composition is held constant at $\phi_0 = 1.3$, the droplet number density n_l varies throughout the domain due to the radial spreading of droplets away from the centerline. In the present quasi-one-dimensional formulation, the strain caused by stagnation results in a radial spreading of the gas phase. Droplet drag forces then generate a radial spreading of the spray, reducing n_l along the centerline. The greater the reduction in n_l, the less spray mass is available for evaporation. A similar effect of fluid dynamics on the local composition was reported by Continillo and Sirignano [9] in the context of laminar counterflow spray flames using a Lagrangian formulation. The wall-stabilized flames reach the lowest values of n_l, which results in lower values of Z_g in the reaction zone, shown in physical space in the upper-right panel of Fig. 4a. Thus, we find that the difference in chemical structure between the wall-stabilized and other regimes can be attributed to the former undergoing locally fuel-leaner combustion. The latter are substantially fuel-richer due to coupling with the fluid dynamics, causing the observed incomplete combustion. In a counterflow configuration, a second reaction zone can form as a diffusion flame between the incomplete combustion products and the counterflowing air, but the presence of the wall precludes this here.

The foregoing discussion demonstrated the sensitivity of the flame structure to the local composition. We now consider the total equivalence ratio ϕ_0 parametrically, as this quantity parametrizes the liquid mass loading and directly affects the composition throughout the flame. In Fig. 5, we show that varying ϕ_0 from fuel-lean to highly fuel-rich values results in a traversal of the previously identified stabilization regimes, as was the case in varying St above. Fuel-lean values of ϕ_0 result in wall-stabilization and little spray penetration of the flame. We note that the result corresponding to $\phi_0 = 1.3$ is the same as that corresponding to St $=$ 0.2 in Fig. 4. Increasing ϕ_0 from fuel-lean values up to 1.35 causes an increase in the flame stand-off distance and an increase in the wall heat flux to a maximum at the transition. The small values of ℓ_p indicate that the entirety of the spray is vaporized and consumed near the reaction zone of the wall-stabilized flame. The continuous increase in $\dot{q}_w$ from globally fuel-lean values of ϕ_0 to a maximum at slightly fuel-rich conditions is in agreement with the prevaporized literature [4].

Beyond $\phi_0 = 1.35$, the flame transitions to the detached regime. The wall heat flux decreases by 50% and decreases further with increasing ϕ_0 across a monotonic transition to injector-stabilization at $\phi_0 = 4.3$. Spray penetration plays a pivotal role under these globally fuel-rich conditions. Whereas decreasing St affects the total spray evaporation through the time scales of individual droplets, increasing ϕ_0 results in an increase in total spray evaporation through n_l. In both cases, the flame stabilizes closer to the injector. However, for the former the spray was seen to be substantially consumed in the flame due to the rapid droplet time scales, whereas in the latter we find that ℓ_p increases from 0.5 in the detached regime at $\phi_0 = 1.5$ to approach 0.9 at $\phi_0 = 5.6$. Consideration of droplet diameter normalized by the initial diameter d_0 in the right panel of Fig. 5b shows that the edge of the spray is in fact nearer to the wall in the injector-stabilized

Please cite this article as: D. Mohaddes and M. Ihme, Wall heat transfer and flame structure transitions in stagnating spray flames, Proceedings of the Combustion Institute, https://doi.org/10.1016/j.proci.2022.08.037

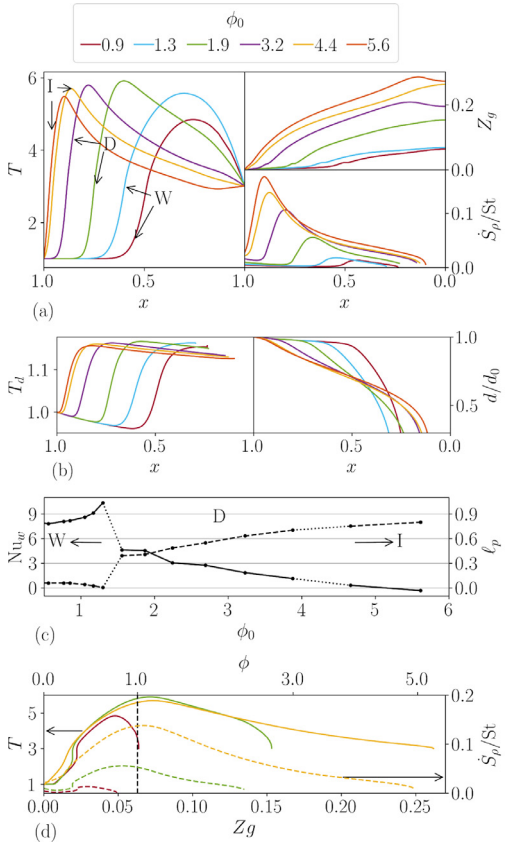

Fig. 5. Parametric dependence on ϕ_0, for Da = 100, St = 0.2 and $T_e = 3.0$. Gas and liquid phase quantities are shown in physical space in (a) and (b), respectively; (c) Nu$_w$ (solid line) and ℓ_p (dashed line), with transitions between regimes shown by dotted lines; (d) results in composition space, with the vertical dotted black line indicating the stoichiometric condition.

cases than those that are wall-stabilized. This substantial penetration of the spray results in reduced gas-phase temperatures downstream of the flame due to the combined effects of heat losses to evaporation and endothermic pyrolysis chemistry. The reduced post-flame temperatures ultimately result in lower wall heat flux, approaching zero at $\phi_0 = 5.6$. Results for higher liquid mass loadings are not presented due to the limitations of the present multicontinuum formulation. Since gas and liquid are injected at a temperature $T = T_d = 1$, the droplet temperature initially decreases due to the latent heat of vaporization, then rises to saturation as the flame is approached, shown in the left panel of Fig. 5b. However, for cases where the spray significantly penetrates the flame, the droplet temperature again decreases due to vaporization and back-coupling to the reduced temperatures in the gas phase.

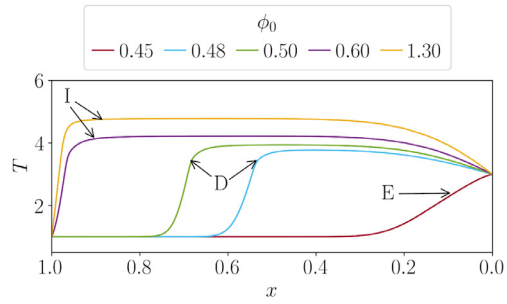

Fig. 6. Parametric dependence on ϕ_0 for gaseous flames, i.e., St $\to$ 0, with Da = 100 and $T_e = 3.0$.

In considering Fig. 4, we showed that St variation indirectly controlled the total mass of fuel available for consumption, affecting Z_g and thereby altering the flame's chemical structure. In Fig. 5a, we show that ϕ_0 directly affects Z_g throughout the flame, as is expected. However, due to spray penetration, we find that the reaction zones of the globally fuel-rich flames considered have substantially fuel-leaner local compositions than the nominal inlet conditions. This effect is most clearly demonstrated in composition space, shown in Fig. 5d. The line corresponding to the wall-stabilized case at $\phi_0 = 0.9$ shows a partially premixed structure: the peak temperature occurs at a gaseous equivalence ratio $\phi = 0.9$, with all spray evaporation occurring at compositions $\phi < 0.9$. By contrast, the detached and injector-stabilized results shown in the figure have characteristics of a diffusion flame structure, in that the peak temperature associated with the reaction zone occurs near stoichiometry, with spray evaporation occurring throughout the range of lean and rich compositions spanned by the system. This behavior is qualitatively similar to that observed for St variation in Fig. 4c. However, the variation in the range of Z_g accessed is substantially greater, since varying ϕ_0 has a direct effect on Z_g, whereas St was shown to have an indirect effect through coupling with the gas-phase fluid dynamics.

As was the case for the parametric variation of Da, we also consider the effect of ϕ_0 variation on the structure of gaseous flames in Fig. 6 for the same values of Da and T_e as were considered in Fig. 5. Comparing the gaseous and spray flames, we find that decreasing ϕ_0 has the same effect of causing the flame to transition from the injector-stabilized to the detached regime, with the transition occurring at a value of ϕ_0 of approximately 0.55. However, unlike in the case of the spray flame, we find that the gaseous flame does not achieve wall-stabilization. Instead, for the present choice of Da and T_e, reduction of ϕ_0 below approximately 0.47 causes the gaseous flame to transition from the detached regime directly to extinction.

Please cite this article as: D. Mohaddes and M. Ihme, Wall heat transfer and flame structure transitions in stagnating spray flames, Proceedings of the Combustion Institute, https://doi.org/10.1016/j.proci.2022.08.037

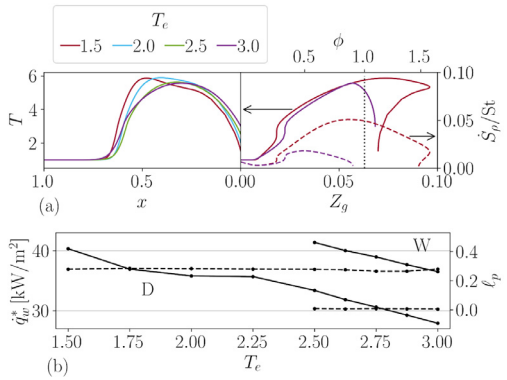

Fig. 7. Parametric dependence on T_e, for St = 0.2, Da = 100, and $\phi_0 = 1.3$. (a) Flame structure in physical and composition space; (b) hysteresis in wall heat flux $\dot{q}_w^*$ and ℓ_p, shown with solid and dashed lines, respectively.

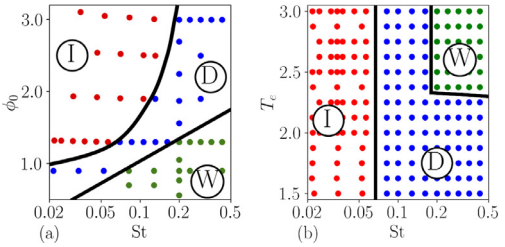

Fig. 8. Flame structure regime diagrams, with approximate boundaries between regimes indicated by black lines. Red, blue and green symbols indicate the injector-stabilized, detached and wall-stabilized flame structures. (a) Da = 100, $T_e = 3.0$; (b) Da = 100, $\phi_0 = 1.3$. (For interpretation of the references to colour in this figure legend, the reader is referred to the web version of this article.)

The analysis presented thus far has considered a constant external wall temperature T_e. T_w varied only due to conjugate effects, which were found to be small in the present configuration: $T_w - T_e < 0.03$ across all cases considered. T_e is of practical importance since systems are often characterized by a known thermal boundary condition. Due to its first-order effect on the thermal gradient at the wall, the effect of wall temperature has been studied in the gas-phase HOQ literature [6]. In Fig. 7, we analyze the effect of T_e on wall heat flux and flame structure. Because of the presence of T_w in the denominator of the definition of Nu_w, we present the wall heat flux in dimensional form in Fig. 7b to clearly demonstrate the effect of the parametric variation. The figure shows that within a given stabilization regime, increasing T_e has the expected effect of decreasing the wall heat flux. However, we find that for $T_e > 3.0$, both detached and wall-stabilized structures can be established, with an associated difference in wall heat flux of up to 30%. Considering the flame structure in physical space in the left panel of Fig. 7a, we see that within a given flame regime, changing T_e has little effect on the topology upstream of the near-wall region. Unlike the other parameter variations considered above, here we find that although the location of the temperature peak changes, the extent of the region with $T > 1$ remains approximately constant in both detached and wall-stabilized regimes. However, the structure in composition space, shown in the right panel, shows qualitatively similar results to those obtained through St variation in the wall-stabilized and detached flame regimes. Quantitatively, the detached regime shows a greater reduction in gaseous temperature in the fuel-rich near-wall region downstream of the reaction zone due to the reduced wall temperature.

As noted in Section 1, counterflow spray flames have been shown to exhibit multiple solutions for certain parameter ranges. In Fig. 7, we demonstrate hysteresis in solution behavior due to the direction of T_e variation. We find that in decreasing T_e, a transition from the wall-stabilized to the detached topology occurs at $T_e = 2.5$, whereas in increasing T_e the flame remains detached throughout the range of T_e considered. The parametric dependence of $\dot{q}_w^*$ on T_e is the same in both flame regimes, and the magnitude of change in $\dot{q}_w^*$ across the transition is thus nearly equal throughout the range where multiple solutions are found. Increased heat loss in the near-wall region from the flame to the wall with reducing T_e results in the wall-stabilized structure only being accessible at large values of T_e. The detached structure, however, can persist at large values of T_e, since the reduced heat loss in the near-wall region causes little change in the upstream flame structure. The presence of hysteresis can have implications for practical purposes. Safety designers and analysts seeking to size components for exposure to wall heat flux should take care to employ the values relevant to the more conservative regime of wall heat flux.

3.2. Regime diagrams

The analysis of Section 3.1 showed that the regimes of flame stabilization could be traversed by varying each of the system parameters considered. However, the physical processes leading to changes in flame structure are themselves coupled. We therefore consider the joint effects of parameter variation through two-dimensional regime diagrams in Fig. 8. We showed in Section 3.1 that ϕ_0 and St both affect the flame structure through $\dot{S}_\rho$. Increased values of ϕ_0 provide a greater total mass of droplets for evaporation, allowing injector stabilization, while increasing St slows droplet evaporation and causes wall-stabilization. These quanti-

Please cite this article as: D. Mohaddes and M. Ihme, Wall heat transfer and flame structure transitions in stagnating spray flames, Proceedings of the Combustion Institute, https://doi.org/10.1016/j.proci.2022.08.037

ties thus have competing effects on the flame structure. In Fig. 8a, we find that highly fuel-rich values of ϕ_0 delay the injector-stabilized/detached transition to large values of St. The injector-stabilized regime is found not to extend into globally fuel-lean conditions in the range of St considered. In the near-injector region, lean mixtures have the same effect as delayed evaporation, precluding stabilization. We find the transition to wall-stabilization to be more sensitive to ϕ_0 than the injector-stabilized/detached transition. Wall-stabilization is only possible if sufficient evaporation has not occurred upstream of the near-wall region to sustain the flame, thus necessitating large values of St to reach the detached/wall-stabilized transition. This was observed in Fig. 6, where for gaseous flames, i.e., $\mathrm{St} \to 0$, wall stabilization could not be achieved. In reducing ϕ_0, the gaseous flames exhibited only a transition from injector stabilization to the detached topology; further reduction in ϕ_0 resulted in the detached flames transitioning directly to extinction.

We noted in the context of Fig. 7 the practical relevance of T_e, and we thus consider the regime diagram for T_e and St in Fig. 8b. To avoid ambiguity in the diagram caused by hysteresis, we traverse the parametric space using St. We find the injector-stabilized/detached transition to be insensitive to T_e. This is expected, since T_e has little effect on the system dynamics outside of the near-wall region, unlike St, which affects the composition throughout the domain by controlling evaporation. The detached/wall-stabilized transition is similarly insensitive at high values of T_e, but we find that wall-stabilization is not achieved for $T_e < 2.3$ in the range of St considered. It is well-established in the HOQ literature [6] that reduced wall temperature increases ℓ_F, and thus we find that at reduced wall temperatures, flame stabilization in the near-wall region is no longer possible and the flame remains in the detached regime.

4. Conclusions

The structure and resulting wall heat transfer of stagnating *n*-dodecane/air spray flames were analyzed using one-dimensional simulations. We showed that three distinct flame structures were possible in this configuration depending on boundary conditions, namely wall-stabilized, detached, and injector-stabilized flames. These structures have important consequences on wall heat flux. We found that reduced and delayed fuel vapor production through evaporation resulted in wall-stabilization, with little spray penetration of the flame. Thus, high values of St and T_e and low values of ϕ_0 and Da tend to result in wall-stabilization. Analysis in composition space showed that flames in this regime have a partially-premixed structure. Detached flames, i.e., stabilized outside the near-wall region, and injector-stabilized flames at globally near-stoichiometric conditions did not achieve complete combustion and produced significant CO compared to wall-stabilized flames of the same global composition due to radial spreading effects coupled to the gas-phase fluid dynamics. Injector-stabilized flames exhibited substantial spray penetration, except when injector stabilization was achieved through reduction of St, which approached prevaporized behavior downstream of the injector.

Transitions between the flame structures were analyzed through parametric variation of boundary conditions, which yielded significant changes in wall heat flux. Flame structure transition was found to exhibit hysteresis when varying T_e, with an associated change in wall heat flux of up to 30%. Wall heat flux varied non-monotonically with all parameters considered except Da due to flame structure transitions and variations within regimes. Through regime diagrams, we analyzed the joint effects of key parameters on the observed flame structures. The understanding of stagnating spray flames provided by this work can serve to inform the design and safety analysis of systems where wall-stagnating spray flames can occur.

Declaration of Competing Interest

The authors declare that they have no known competing financial interests or personal relationships that could have appeared to influence the work reported in this paper.

Acknowledgments

Financial support from The Boeing Company under grant number 134708 [IC2017-2182] and ONR under award number N68335-19-C-0177 is gratefully acknowledged.

References

[1] G. Kats, J.B. Greenberg, Stagnation-point polydisperse spray flame ignition, Combust. Theory Model. 23 (5) (2019) 771–797, doi:10.1080/13647830.2019.1589580.
[2] D. Mohaddes, P. Boettcher, M. Ihme, Hot surface ignition of a wall-impinging fuel spray: modeling and analysis using large-eddy simulation, Combust. Flame 228 (2021) 443–456, doi:10.1016/j.combustflame.2021.02.025.
[3] G. Bruneaux, Combustion structure of free and wall-impinging diesel jets by simultaneous laser-induced fluorescence of formaldehyde, poly-aromatic hydrocarbons, and hydroxides, Int. J. Engine Res. 9 (3) (2008) 249–265, doi:10.1243/14680874JER00108.
[4] A. Wehrfritz, H. Wang, E.R. Hawkes, Y. Gao, T. Lu, Wall-impinging laminar premixed n-dodecane

flames under autoignitive conditions, Proc. Combust. Inst. 37 (2) (2019) 1647–1654, doi:10.1016/J.PROCI.2018.06.118.
[5] A. Dreizler, B. Böhm, Advanced laser diagnostics for an improved understanding of premixed flame-wall interactions, Proc. Combust. Inst. 35 (1) (2015) 37–64, doi:10.1016/j.proci.2014.08.014.
[6] Y. Luo, C. Strassacker, X. Wen, Z. Sun, U. Maas, C. Hasse, Strain rate effects on head-on quenching of laminar premixed methane-air flames, Flow Turbul. Combust. 106 (2) (2021) 631–647, doi:10.1007/s10494-020-00179-1.
[7] M. Mann, C. Jainski, M. Euler, B. Böhm, A. Dreizler, Transient flame-wall interactions: experimental analysis using spectroscopic temperature and CO concentration measurements, Combust. Flame 161 (9) (2014) 2371–2386, doi:10.1016/j.combustflame.2014.02.008.
[8] E. Gutheil, W.A. Sirignano, Counterflow spray combustion modeling with detailed transport and detailed chemistry, Combust. Flame 113 (1–2) (1998) 92–105, doi:10.1016/S0010-2180(97)00192-2.
[9] G. Continillo, W.A. Sirignano, Counterflow spray combustion modeling, Combust. Flame 81 (3–4) (1990) 325–340, doi:10.1016/0010-2180(90)90029-Q.
[10] W. Xie, W. Wu, Z. Ren, H. Liu, M. Ihme, Effects of evaporation on chemical reactions in counterflow spray flames, Phys. Fluids 33 (6) (2021) 065115, doi:10.1063/5.0046313.
[11] W. Xie, P.B. Govindaraju, Z. Ren, M. Ihme, Structural analysis and regime diagrams of laminar counterflow spray flames with low-temperature chemistry, Proc. Combust. Inst. 38 (September) (2021) 3193–3200, doi:10.1016/j.proci.2020.06.274.
[12] A. Vié, B. Franzelli, Y. Gao, T. Lu, H. Wang, M. Ihme, Analysis of segregation and bifurcation in turbulent spray flames: a 3D counterflow configuration, Proc. Combust. Inst. 35 (2) (2015) 1675–1683, doi:10.1016/J.PROCI.2014.06.083.
[13] Federal Aviation Administration, Powerplant Installation and Propulsion System Component Fire Protection Test Methods, Standards and Criteria, Technical Report AC 20-135, 2018.
[14] B. Franzelli, B. Fiorina, N. Darabiha, A tabulated chemistry method for spray combustion, Proc. Combust. Inst. 34 (1) (2013) 1659–1666, doi:10.1016/j.proci.2012.06.013.
[15] N. Darabiha, F. Lacas, J.C. Rolon, S. Candel, Laminar counterflow spray diffusion flames: a comparison between experimental results and complex chemistry calculations, Combust. Flame 95 (3) (1993) 261–275, doi:10.1016/0010-2180(93)90131-L.
[16] E. Radenac, J. Gressier, P. Millan, Methodology of numerical coupling for transient conjugate heat transfer, Comput. Fluids 100 (2014) 95–107, doi:10.1016/j.compfluid.2014.05.006.
[17] D.G. Goodwin, R.L. Speth, H.K. Moffat, B.W. Weber, Cantera: an object-oriented software toolkit for chemical kinetics, thermodynamics, and transport processes, 2017, (https://www.cantera.org), Version 2.4.0. 10.5281/zenodo.170284
[18] A. Singh, M. Mann, T. Kissel, J. Brübach, A. Dreizler, Simultaneous measurements of temperature and CO concentration in stagnation stabilized flames, Flow Turbul. Combust. 90 (4) (2013) 723–739, doi:10.1007/s10494-011-9384-6.
[19] T. Yao, Y. Pei, B.-J. Zhong, S. Som, T. Lu, K.H. Luo, A compact skeletal mechanism for n-dodecane with optimized semi-global low-temperature chemistry for diesel engine simulations, Fuel 191 (2017) 339–349, doi:10.1016/J.FUEL.2016.11.083.
[20] D. Vlachos, L. Schmidt, R. Aris, Ignition and extinction of flames near surfaces: combustion of H_2 in air, Combust. Flame 95 (3) (1993) 313–335, doi:10.1016/0010-2180(93)90135-P.
[21] D. Mohaddes, M. Ihme, On the hot surface ignition of a wall-stagnating spray flame, Combust. Flame 240 (2022) 111988, doi:10.1016/j.combustflame.2022.111988.

Please cite this article as: D. Mohaddes and M. Ihme, Wall heat transfer and flame structure transitions in stagnating spray flames, Proceedings of the Combustion Institute, https://doi.org/10.1016/j.proci.2022.08.037